

Ring current modeling in a realistic magnetic field configuration

M.-C. Fok

Universities Space Research Association, Space Sciences Laboratory, NASA/MSFC, Huntsville, AL

T. E. Moore

Space Sciences Laboratory, NASA/Marshall Space Flight Center, Huntsville, AL

Abstract. A 3-dimensional kinetic model has been developed to study the dynamics of the storm time ring current in a dipole magnetic field. In this paper, the ring current model is extended to include a realistic, time-varying magnetic field model. The magnetic field is expressed as the cross product of the gradients of two Euler potentials and the bounce-averaged particle drifts are calculated in the Euler potential coordinates. A dipolarization event is modeled by collapsing a tail-like magnetosphere to a dipole-like configuration. Our model is able to simulate the sudden enhancements in the ring current ion fluxes and the corresponding ionospheric precipitation during the substorm expansion.

Introduction

This work is an extension of our previous study in ring current modeling. We have developed a 3-dimensional (in configuration space) model that solves the kinetic equation of the distribution functions of ring current ion species, considering arbitrary pitch angle distribution (PAD) and losses along drift paths. The magnetic field was assumed to be a dipole. The model has been used to simulate the recovery phase of a great storm [Fok *et al.*, 1995] and the main phase of a moderate storm [Fok *et al.*, 1996]. The calculated ion fluxes, in general, agreed well with the measurements from the AMPTE/CCE (Active Magnetospheric Particle Tracer Explorers/Charge Composition Explorer) satellite. However, with the assumption of a dipole field, the model is valid only in the inner magnetosphere ($L \lesssim 7$), where the magnetic field is not much different from a dipole. Moreover, a constant magnetic field cannot be applied to simulate the rapid varying substorm dynamics, but a time-dependent model is necessary.

Earlier work has been done in modeling the ring current in a non-dipolar magnetic field. The model employed by Chen *et al.* [1994] is a superposition of a uniform southward field ($\Delta B = 14.474$ nT) to a magnetic dipole. Their model is a bit more realistic than a pure dipole field and it contains a quasi-magnetopause at the boundary between closed and open field lines. Takahashi and Iyemori [1989] calculated the particle trajectories in a magnetic field model of Mead-Fairfield and found day-night asymmetry in the flow patterns due to the asymmetry in the gradient and curvature drifts. The Rice Convection Model (RCM) [Harel *et al.*, 1981] used the analytic magnetic field model of Olson and Pfitzer [1974]. In order to simulate the substorm associated magnetic field variations, the magnetic field produced by a time-varying "substorm current

loop" was added to the Olson and Pfitzer model. In RCM, the bounce-averaged drifts were calculated with the assumption that the particle PAD is isotropic. In this paper, our ring current model is extended to include a realistic, activity-dependent magnetic field model, more specifically, the Tsyganenko 89 model [Tsyganenko, 1989]. The storm on May 2, 1986, which has been studied previously [Fok *et al.*, 1996], is simulated using our improved model. In the following, the derivation of the bounce-averaged drift of particles with arbitrary pitch angles, in an arbitrary magnetic field configuration, will be given. We will then present the results of ion flux enhancements and the corresponding precipitation at the ionosphere as we model a dipolarization event.

Bounce-averaged Drift in Euler Potential Coordinates

Northrop [1963] has shown that the bounce-averaged drift of a charge particle in a magnetic field can be represented by the velocities in the Euler potential coordinates, (α, β) , as:

$$\langle \dot{\alpha} \rangle = -\frac{1}{q} \frac{\partial H}{\partial \beta}, \quad \langle \dot{\beta} \rangle = \frac{1}{q} \frac{\partial H}{\partial \alpha} \quad (1)$$

where H is defined as:

$$H = \sqrt{p^2 c^2 + m_0^2 c^4} + q\Phi + q\alpha \partial \beta / \partial t \quad (2)$$

where Φ is the cross-tail potential. α and β are chosen such that vector potential $\mathbf{A} = \alpha \nabla \beta$ and $\mathbf{B} = \nabla \alpha \times \nabla \beta$. These Euler potentials are used to specify a field line, therefore they have to be constant along the line of force.

In finding an appropriate set of (α, β) , it is convenient to first choose two general coordinates, C_1 and C_2 , which are also constants along a field line and can be used to specify that field line, but $C_1 \nabla C_2$ is not equal to \mathbf{A} . The lines of force are thus the intersections of two families of surfaces given by $C_1 = \text{constant}$ and $C_2 = \text{constant}$. Let us define a quantity ξ , such that

$$\xi = B / |\nabla C_1 \times \nabla C_2| \quad (3)$$

Northrop [1963] has shown that ξ is a constant along a field line, and α and β can be obtained by letting $\beta = C_2$, α is then given by $\alpha = \int \xi dC_1$. In this study, we take $C_1 = \lambda_i$, $C_2 = \phi_i$, in which λ_i and ϕ_i are the magnetic latitude and magnetic local time, respectively, of the ionospheric foot point of the field line. In other words, the ionospheric foot point is used to label a field line instead of the equatorial crossing point. As the magnetosphere is compressed or expanded in response to the solar wind and/or internal instabilities, the equatorial crossing of a field line at a particular local time is no longer a constant. However, field lines can be regarded as rooted at the ionosphere, where the magnetic

variation is very small. Thus it is more convenient to identify a field line by its foot point in the ionosphere. If the magnetic field is assumed to be a pure dipole in the ionosphere, ξ is found equal to $M_E \sin 2\lambda_i / r_i$, where M_E is the Earth's magnetic dipole moment; r_i is the radial distance of the ionospheric foot point of a field line. In this study, $r_i = 1.126$ earth radii (~ 800 km altitude) has been chosen. The derivation of ξ is given in the Appendix. With ξ given as above, α can be easily found by integrating ξ over λ_i and has the expression:

$$\alpha = -M_E \cos 2\lambda_i / 2r_i \quad (4)$$

Considering the rotation of the Earth and assuming that the rotation axis is aligned with the magnetic axis, the last term in the expression of H in (2) is given by:

$$q\alpha \partial\beta / \partial t = q\alpha \partial\phi_i / \partial t = q\alpha\Omega \quad (5)$$

where Ω is the angular velocity of the rotation of the Earth. H thus can be rewritten as:

$$H = \sqrt{p^2 c^2 + m_0^2 c^4} + q\Phi + q\alpha\Omega \quad (6)$$

In calculating the particle drift from (1), the three terms in H correspond to the gradient-curvature drift, the electric drift due to the cross-tail potential, and the corotation with the Earth. The compression and expansion of the magnetosphere during substorms do not yield any non-zero value of $\partial\phi_i / \partial t$ because we have assumed that the ionospheric foot points of field lines are unchanged due to substorm activities. The substorm induced electric field and the resulting bounce-averaged drift are treated implicitly by continuously changing the gradient-curvature drift according to the instantaneous magnetic configuration. At the same time, the mapping of particle distribution from the ionospheric grids to the magnetosphere is adjusted correspondingly.

The bounce-averaged drifts in (1) can be written in terms of λ_i and ϕ_i . Since α is independent of ϕ_i , we have

$$\frac{\partial}{\partial\alpha} = \frac{1}{\xi} \frac{\partial}{\partial\lambda_i}, \quad \dot{\alpha} = \xi \dot{\lambda}_i \quad (7)$$

The bounce-averaged drift in (λ_i, ϕ_i) coordinates is thus:

$$\langle \dot{\lambda}_i \rangle = -\frac{1}{q\xi} \frac{\partial H}{\partial\phi_i}, \quad \langle \dot{\phi}_i \rangle = \frac{1}{q\xi} \frac{\partial H}{\partial\lambda_i} \quad (8)$$

As shown in (6) and (8), the bounce-averaged magnetic drift can be calculated if the variations of the particle momentum (p) in the Euler potential coordinates are given. However, in our model, particles are identified by their adiabatic invariants: M (relativistic magnetic moment) and K ($K = J/\sqrt{8m_0M}$). Our next task is to calculate p for given M and K . For a particular K value and a field line of the Tsyganenko model specified by λ_i and ϕ_i , the magnetic field at the mirror point, B_m , can be obtained by

$$K = J/\sqrt{8m_0M} = \int_{s_m}^{s_m'} (B_m - B)^{1/2} ds \quad (9)$$

Solving (9) for B_m is not trivial. It requires field line tracing and integration, and numerical technique to solve an implicit function. Once $B_m(\lambda_i, \phi_i, K)$ is calculated, p can be easily found as follows:

$$M = p_{\perp}^2 / 2m_0 B = p^2 / 2m_0 B_m \quad (10)$$

$$p^2(\lambda_i, \phi_i, M, K) = 2m_0 B_m M \quad (11)$$

With the bounce-averaged drift given by (8), the temporal variation of a ring current species can be calculated by solving the following kinetic equation:

$$\frac{\partial \bar{f}_s}{\partial t} + \langle \dot{\lambda}_i \rangle \frac{\partial \bar{f}_s}{\partial \lambda_i} + \langle \dot{\phi}_i \rangle \frac{\partial \bar{f}_s}{\partial \phi_i} = -v\sigma_s \langle n_H \rangle \bar{f}_s - \left(\frac{\bar{f}_s}{0.5\tau_b} \right)_{\text{loss cone}} \quad (12)$$

where $\bar{f}_s = \bar{f}_s(t, \lambda_i, \phi_i, M, K)$, is the average distribution function on the field line between mirror points. σ_s is the cross section for charge exchange of species s with the neutral hydrogen and n_H is the hydrogen density. τ_b is the bounce period. The second term on the right hand side of (12) is applied only to particles with pitch angle inside the loss cone, which is defined at 800 km. In this study, only loss due to charge exchange with the neutral hydrogen and loss at the loss cone are considered.

Enhancement in Equatorial and Precipitation Fluxes During Dipolarization

We have previously simulated a series of substorm events by adding to the particle drift velocity the induced electric drift [Fok *et al.*, 1996]. However, the gradient-curvature drifts were calculated in a constant dipole field. The problem will be revisited with the realistic, time-dependent magnetic configuration and the corresponding drifts. The main phase of the magnetic storm on May 2, 1986 is modeled. As in Fok *et al.* [1996], the Tsyganenko model [Tsyganenko, 1989, EXT89AE routine] is employed to simulate the shape of the magnetosphere associated with six levels of the AE index. Figure 1, which is essentially the lower panel of Figure 5 in Fok *et al.* [1996], plots the simulated levels of the Tsyganenko model as a function of UT on May 2, 1986.

The ring current H^+ fluxes are calculated during the storm. The initial fluxes are given by the quiet time measurements by AMPTE/CCE [Sheldon and Hamilton, 1993]. The instantaneous boundary fluxes near the nightside geosynchronous orbit are obtained by interpolation in time of measurements from two CCE orbits at 0800 and 2400 UT. The pitch angle-averaged differential fluxes at the equator at a substorm onset (marked as (a) in Figure 1) and at the end of the expansion phase (marked as (b) in Figure 1) are displayed in Plate 1. Ions with energies of 1–5, 5–40 and 40–300 keV are represented by red, green and blue, respectively. The color bars show the intensity levels of the fluxes. White color in the plot indicates that the mean fluxes in all three energy ranges are over $5 \times 10^4 \text{ cm}^{-2} \text{ s}^{-1} \text{ sr}^{-1} \text{ keV}^{-1}$.

Plate 1 exhibits a typical spatial distribution of the ring current ion energy spectra during the active period. Low and medium energy ions are injected from the tail (yellow region on the

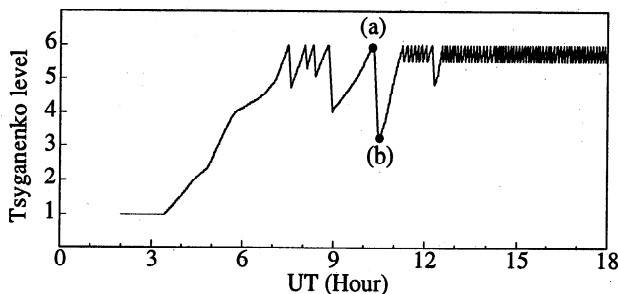


Figure 1. Simulated levels of Tsyganenko model (EXT89AE) on May 2, 1986. The two times at which equatorial and precipitating fluxes will be shown in Plates 1 and 2 are marked as (a) and (b).

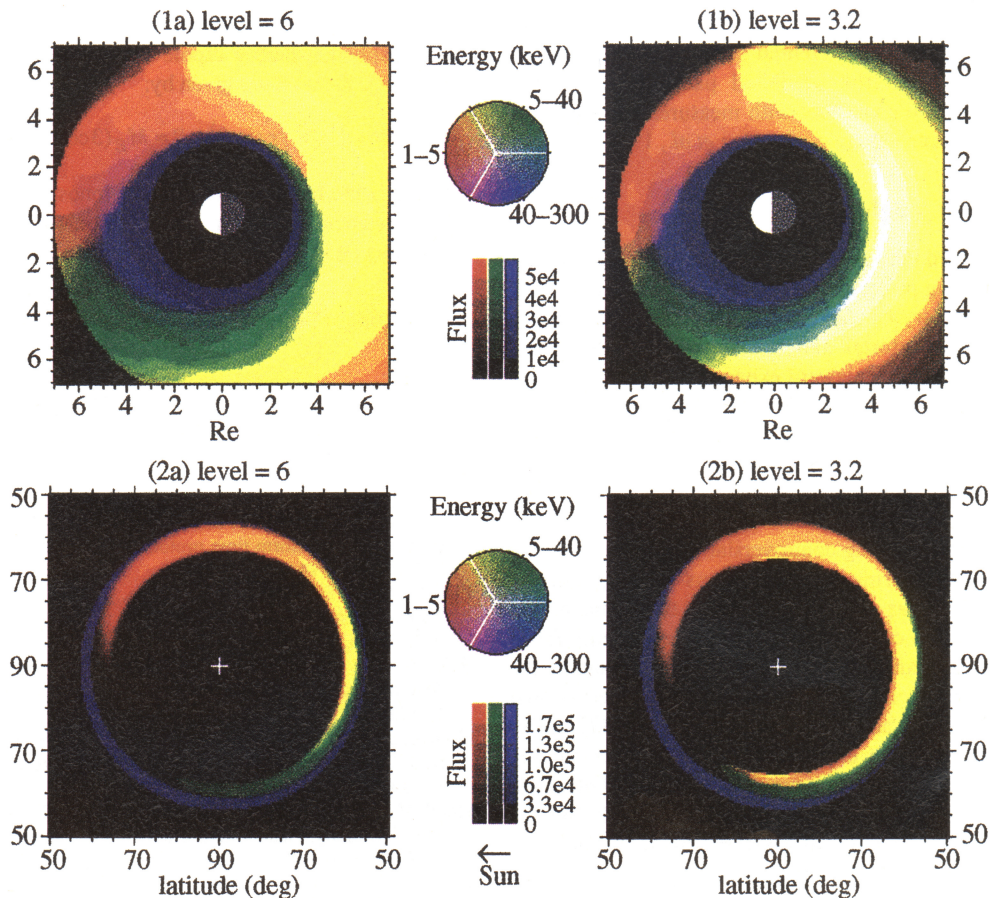


Plate 1, 2. Plate 1: equatorial H⁺ fluxes (cm⁻²s⁻¹sr⁻¹keV⁻¹) and Plate 2: precipitating H⁺ fluxes (cm⁻²s⁻¹keV⁻¹) at (a) substorm onset, and (b) at the end of the expansion phase. Ions with energies 1–5, 5–40 and 40–300 keV are represented in red, green and blue, respectively. The color bars indicate the minimum and maximum flux levels shown in the plates.

nightside). Corotation moves low energy ions to the dayside through dawn (red region in the prenoon sector). Westward gradient-curvature drift dominates the motion of ions with higher energies and they reach the dayside through dusk (blue region across dusk and in the postnoon sector). The blue tear drop shape area represents the region dominated only by high energy (40–300 keV) ions. This is the region of closed drift path for low energy ions. Therefore, in this inner part of the magnetosphere, the charge exchange loss of low energy ions cannot be compensated by injection from the tail.

In Plate 1, the outer bound of the model threads through field lines to the ionosphere at 65.4° latitude, while the inner boundary corresponds to 41.4° at the ionosphere. At the substorm onset (Plate 1a), the magnetosphere is expanded corresponding to Tsyganenko level 6. In 12 minutes, the magnetosphere collapses to a lower level of 3.2 (Plate 1b). At that moment, strong ion fluxes are seen on the nightside at 4–6 earth radii (white and light yellow fringe). This sudden enhancement in the nightside ion fluxes is a consequence of particle energization during substorm expansion. The energy (or momentum) of a particle gyrating along a stretched field line will increase when the field line relaxes to more dipole-like, in order to conserve the first and second adiabatic invariants. The increase in p will increase the differential flux, j_s ($j_s = p^2 f_s$), since f_s is a Liouville-invariant quantity.

Under the assumption of constant flux along a field line, we are able to calculate ion fluxes at any location in the

magnetosphere. The pitch angle-integrated precipitating fluxes (in cm⁻²s⁻¹keV⁻¹) at 800 km before and after the substorm expansion are calculated and plotted in Plate 2. Fluxes are displayed as a function of latitude and magnetic local time with the sun to the left. As in Plate 1, ions at low, medium and high energies are represented by red, green and blue, respectively. The H⁺ precipitation shown in Plate 2 is basically an inside out mapping of the equatorial fluxes displayed in Plate 1. However, the precipitation intensity shows a stronger day-night asymmetry than the fluxes at the equator. The precipitation on the nightside is stronger because the nightside earthward convection continuously pushes particles toward the loss cone by transporting them to lower L shells and lowering the mirror point altitudes. Similar to the case of particle energy, the pitch angle of an ion encircling a field line varies when the field line is elongating or collapsing. During substorm growth phase, particles bounce along extending field lines and thus mirror at high altitudes. As a consequence, the precipitation to the ionosphere is weakened. At the end of the growth phase (Plate 2a), precipitation is found only in a narrow range of latitude. In contrast, during field line relaxation, the pitch angles of ions decrease, as well as the mirror altitudes. As shown in Plate 2b, the region of precipitation extends poleward at the end of the expansion phase. In fact, dipolarization events have been found to be closely connected with sudden enhancements in precipitating ion and electron fluxes at the ionosphere [Shepherd *et al.*, 1980]. The calculated precipitating fluxes in Plate 2 are in

the order of $10^5 \text{ cm}^{-2}\text{s}^{-1}\text{keV}^{-1}$. With a mean energy approximately 30 keV, the differential energy flux is about $10^6 \text{ eV}/(\text{cm}^2\cdot\text{s}\cdot\text{sr}\cdot\text{eV})$. Both the predicted particle and energy precipitating fluxes are consistent with measurements at active times by the DMSP satellites [e.g., *Sanchez et al.*, 1996].

Discussion and Conclusions

We have simulated the variations of the ring current H^+ fluxes and the corresponding precipitation during a dipolarization event, in a realistic, time-varying magnetic field model. The sudden increases in both equatorial and ionospheric ion fluxes are reproduced, as well as the poleward expansion of the ion aurora. In the particular case we have modeled, the Tsyganenko magnetic field level drops from 6 to 3.2. In a complete collapse of the magnetosphere (from level 6 to level 1), particle flux enhancements should be more pronounced than those shown in Plates 1 and 2.

It has been a long-standing controversial issue of the relative efficiency between storms and substorms in ring current formation [e.g., *Gonzalez et al.*, 1994]. From the results of this study, it is tempting to conclude that the induced electric fields associated with dipolarization are crucially important in the injection of the ring current. However, new observational [*Iyemori and Rao*, 1996] and modeling [*Wolf et al.*, 1997] studies have shown that substorm expansion has little effect on ring current intensification. We have previously shown [*Fok et al.*, 1996] that the decrease of the total electric field during the growth phases between a series of substorm dipolarizations, can outweigh the effects of the increased fields during the dipolarizations. As a result, a more robust ring current was actually produced when the substorm dipolarizations were omitted from the simulation. As in the present study, however, boundary condition at the nightside was obtained by interpolation of AMPTE/CCE measurements every 16 hours. These "averaged" fluxes cannot fully represent the substantial flux dropout during the growth phase [*Sauvaud et al.*, 1996] and the enhanced particle injection during the rapid expansion phase. In future work, a substorm phase-dependent outer boundary condition will be implemented to better connect the dynamics of the mid-tail to the inner magnetosphere. A more definitive assessment of the relative importance of induced and convective electric fields can then be given.

Even though this work is a big leap forward of our effort in ring current modeling that includes a realistic magnetic field model, we still have not treated the electric and magnetic fields self-consistently. In future, we plan to develop a comprehensive ring current model, which solves a complete set of physical equations self-consistently, by coupling our model, the Rice Convection Model, and a friction-code algorithm.

In conclusion, we have modeled the distribution of the ring current ions of arbitrary pitch angle distribution in a realistic, activity-dependent magnetic field configuration. Our improved model is able to simulate the enhancements in the ring current ion fluxes and the associated ion precipitation in the ionosphere during a dipolarization event.

Appendix: The Derivation of ξ

As shown in (3),

$$\xi = B/|\nabla\lambda_i \times \nabla\phi_i| \quad (\text{A1})$$

ξ is constant along a field line, therefore it can be evaluated at

any point on the line of force. It is convenient to calculate ξ at the ionosphere where a dipole field is assumed. In a dipolar ionosphere, λ_i and B are given by:

$$\lambda_i = \cos^{-1}\left(\sqrt{r_i/r} \sin\theta\right), \quad B = M_E(3\cos^2\theta + 1)^{1/2}/r^3 \quad (\text{A2})$$

where r_i is the radial distance of the ionosphere; r and θ are the radial distance and polar angle of the spherical coordinates. Combining (A1) and (A2), we have

$$|\nabla\lambda_i \times \nabla\phi_i| = \frac{\sqrt{1+3\cos^2\theta}}{2r^2 \sin\theta} \sqrt{\frac{r_i}{r-r_i \sin^2\theta}} \quad \text{and} \quad (\text{A3})$$

$$\xi = M_E \sin 2\lambda_i / r_i \quad (\text{A4})$$

References

- Chen, M. W., L. R. Lyons, and M. Schulz, Simulations of phase space distributions of storm time proton ring current, *J. Geophys. Res.*, **99**, 5745-5759, 1994.
- Fok, M.-C., T. E. Moore, J. U. Kozyra, G. C. Ho, and D. C. Hamilton, Three-dimensional ring current decay model, *J. Geophys. Res.*, **96**, 9632, 1995.
- Fok, M.-C., T. E. Moore, and M. E. Greenspan, Ring current development during storm main phase, *J. Geophys. Res.*, **101**, 15,311-15,322, 1996.
- Gonzalez, W. D., J. A. Joselyn, Y. Kamide, H. W. Kroehl, G. Rostoker, B. T. Tsurutani, and V. M. Vasylunas, What is a geomagnetic storm, *J. Geophys. Res.*, **99**, 5771-5792, 1994.
- Harel, M., R. A. Wolf, P. H. Reiff, R. W. Spiro, W. J. Burke, F. J. Rich, and M. Smiddy, Quantitative simulation of a magnetospheric substorm 1. Model logic and overview, *J. Geophys. Res.*, **86**, 2217-2241, 1981.
- Iyemori, T., and D. R. K. Rao, Decay of the Dst field of geomagnetic disturbance after substorm onset and its implication to storm-substorm relation, *Ann. Geophys.*, **14**, 608-618, 1996.
- Northrop, T. G., *The Adiabatic Motion Of Charged Particles*, John Wiley & Sons, New York, 1963.
- Olson, W. P., and K. A. Pfitzer, A quantitative model of the magnetospheric magnetic field, *J. Geophys. Res.*, **79**, 3739-3748, 1974.
- Sanchez, E. R., J. M. Ruohoniemi, C.-I. Meng, and E. Friis-Christensen, Toward an observational synthesis of substorm models: Precipitation regions and high-latitude convection reversals observed in the nightside auroral oval by DMSP satellites and HF radars, *J. Geophys. Res.*, **101**, 19,801-19,837, 1996.
- Sauvaud, J. A., T. Beutier, and D. Delcourt, On the origin of flux dropouts near geosynchronous orbit during the growth phase of substorms 1. Betatron effects, *J. Geophys. Res.*, **101**, 19,911-19,919, 1996.
- Sheldon, R. B., and D. C. Hamilton, Ion transport and loss in the earth's quiet ring current 1. Data and standard model, *J. Geophys. Res.*, **98**, 13,491-13,508, 1993.
- Shepherd, G. G., R. Bostrom, H. Derblom, C.-G. Falthammar, R. Gendrin, K. Kaila, A. Korth, A. Pedersen, R. Pellinen, and G. Wrenn, Plasma and field signatures of poleward propagating auroral precipitation observed at the foot of the Geos 2 field line, *J. Geophys. Res.*, **85**, 4587-4601, 1980.
- Takahashi, S., and T. Iyemori, Three-dimensional tracing of charged particle trajectories in a realistic magnetic model, *J. Geophys. Res.*, **94**, 5505-5509, 1989.
- Tsyganenko, N. A., A magnetospheric magnetic field model with a warped tail current sheet, *Planet. Space Sci.*, **37**, 5-20, 1989.
- Wolf, R. A., J. W. Freeman, Jr., B. A. Hausman, R. W. Spiro, R. V. Hilmner, and R. L. Lambour, Modeling convection effects in magnetic storm, *J. Geophys. Res.*, in press, 1997.

M.-C. Fok, USRA, Space Sciences Laboratory, ES83, NASA/MSFC, Huntsville, AL 35812. (E-mail: fok@msfc.nasa.gov)

T. E. Moore, Space Science Laboratory, ES83, NASA/MSFC, Huntsville, AL 35812. (E-mail: t.e.moore@msfc.nasa.gov)

(Received December 17, 1996; revised March 31, 1997; accepted April 21, 1997.)